

Spectroscopic comprehension of Mott-Hubbard insulator to negative charge transfer metal transition in $\text{LaNi}_x\text{V}_{1-x}\text{O}_3$ thin films

Anupam Jana ^{1,*}, Sophia Sahoo,¹ Sourav Chowdhury,¹ Arup Kumar Mandal,¹ Santosh Bimli,² Rupesh S. Devan,² R. J. Choudhary,^{1,†} D. M. Phase,¹ and A. K. Raychaudhuri³

¹UGC DAE Consortium for Scientific Research, Indore-452001, India

²Department of Metallurgy Engineering and Materials Science,

Indian Institute of Technology Indore, Khandwa Road, Simrol, Indore, 453552, India

³CSIR- Central Glass and Ceramic Research Institute, Kolkata -700032, India



(Received 8 June 2021; accepted 21 October 2022; published 14 November 2022)

The room-temperature (300 K) electronic structure of pulsed laser deposited $\text{LaNi}_x\text{V}_{1-x}\text{O}_3$ thin films has been demonstrated. The substitution of early-transition metal (TM) V in LaVO_3 thin films with late-TM Ni leads to the decreasing in out-of-plane lattice parameter. Doping of Ni does not alter the formal valence state of Ni and V in $\text{LaNi}_x\text{V}_{1-x}\text{O}_3$ thin films, divulging the absence of carrier doping into the system. The valence-band spectrum is observed to comprise incoherent structure owing to the localized V $3d$ band along with the coherent structure at Fermi level. With increase in Ni concentration, the weight of the coherent feature increases, which divulges its origin to the Ni $3d$ -O $2p$ hybridized band. The shift of Ni $3d$ -O $2p$ hybridized band towards higher energy in Ni-doped LaVO_3 films compared to the LaNiO_3 film endorses the modification in ligand to metal charge transfer (CT) energy. The Ni doping in Mott-Hubbard insulator LaVO_3 leads to the closure of the Mott-Hubbard gap by building of spectral weight that provides the delocalized electrons for conduction. A transition from bandwidth control Mott-Hubbard insulator LaVO_3 to negative CT metallic character in LaNiO_3 film is observed. The study reveals that unlike in Mott-Hubbard insulators, where the strong Coulomb interaction between the $3d$ electrons decides the electronic structure of the system, CT energy can deliver an additional degree of freedom to optimize material properties in Ni-doped LaVO_3 films.

DOI: [10.1103/PhysRevB.106.205123](https://doi.org/10.1103/PhysRevB.106.205123)

I. INTRODUCTION

Since the discovery of colossal magnetoresistance (CMR) phenomenon in perovskite manganites, the high- T_c superconductors in cuprates, filling/bandwidth control metal to insulator transition (MIT) has escalated the research on the doped perovskite in transition-metal oxide (TMO) systems [1–5]. In this aspect, $\text{LaNi}_x\text{V}_{1-x}\text{O}_3$ perovskite oxides would be very interesting because the parent compounds LaVO_3 (LVO) and LaNiO_3 (LNO) are electronically and electrically very different from each other. LVO displays the Mott-Hubbard type insulating character [6], while LNO shows the metallic nature at room temperature (RT) [7]. It can provide an interesting occurrence of insulator to metal transition as one increases x in $\text{LaNi}_x\text{V}_{1-x}\text{O}_3$ and traverses a path between the end members of the series from paramagnetic Mott-Hubbard insulating LVO to Pauli paramagnetic metallic LNO. Besides, in $\text{LaNi}_x\text{V}_{1-x}\text{O}_3$, the Ni^{3+} ($3d^7$) and V^{3+} ($3d^2$) ions have different electron occupancies, which may reveal the competing spin and charge interactions and alter the various electron correlation energies leading to unusual physical properties.

The primitive cell of bulk LVO is orthorhombic with lattice parameters $a = 5.55548 \text{ \AA}$, $b = 7.84868 \text{ \AA}$, and $c = 5.55349 \text{ \AA}$ [8]. The strong electron correlation in LVO enforces the electron to be localized to their lattice site; consequently, an insulating state emerges at RT and persists down to the low temperature (LT) [9,10]. LVO exhibits a structural transition from orthorhombic to monoclinic below 141 K and magnetic transition from paramagnetic to antiferromagnetic below 143 K [8,11]. Unlike isoelectronic V_2O_3 [4,12], structural transition in LVO is not accompanied with MIT; however, conductivity is strongly suppressed in the monoclinic state of LVO due to the dispersionless nature of the conduction band [10,13]. On the other hand, the crystal structure of LNO is rhombohedral with Pauli paramagnetic behavior. Unlike other nickelates, LNO does not show a MIT and remains metallic down to 1.5 K [14], although the T^2 dependence of resistivity at LT, heat capacity studies, and a Pauli paramagnetic-like susceptibility suggest an enhanced electron effective mass ($m^* \sim 10 m_0$), which are attributed to strongly correlated Ni $3d e_g$ electrons close to a MIT [15–17]. Therefore, in these compounds, various parameters such as electron-electron correlations, bandwidth, O $2p$ -TM $3d$ hybridization strength, charge transfer energy, band occupancy, etc. are some crucial microstructural parameters which tremendously influence the electrical, electronic, magnetic, specific heat, and various other physical properties [18–21].

Previous studies on doped perovskite TMOs, such as $\text{LaNi}_{1-x}\text{M}_x\text{O}_3$ ($M = \text{Cr, Mn, Fe, or Co}$) compounds [22–25]

*Present address: CNR-IOM, TASC Laboratory in Area Science Park, 34139 Trieste, Italy, International Centre for Theoretical Physics (ICTP), 34100 Trieste, Italy.

†ram@csr.res.in

suggested that there was a characteristic critical composition (x_c) which brings in the transition from the metallic to non-metallic state in the series [26]. Interestingly, x_c was found to be different for different TM elements, which indicated that the effects of electronic disorder also have crucial role in MIT [23]. Moreover, the electronic structure study in these doped systems also suggests that MIT is due to the potential mismatch between the substituent metal ion and Ni^{3+} ion, which causes the transferring of hole states from near-Fermi level (E_F) to an energy position above E_F [24]. The substitution of TM with different ionic radius alters the TM-O-TM bond topology leading to the modification in electronic bandwidth (W), which also has an important role in controlling MIT in doped systems [14,26–29]. Therefore, the mixed perovskite systems are the suitable ground to explore the MIT and its electronic manifestation to decipher the role of critical charge-carrier densities, disorders, as well as structural transition.

It should be noted here that these dopings in LNO were mostly by the middle/late M transition metals, with end members LaMO_3 being mostly charge transfer insulators [30]. However, doping by an early-TM element like V, with end member LaVO_3 being a Mott-Hubbard insulator, is not studied. Therefore, in the present study we have investigated the electronic structure of $\text{LaNi}_x\text{V}_{1-x}\text{O}_3$ ($x = 0, 0.2, 0.4, 0.5, 0.8$, and 1.0) thin films at RT using photoemission and absorption spectroscopy techniques, where the substitution of V with Ni not only enhances the density of states (DOS) at the E_F , but also induces electronic disorder and the charge transfer between the two TM ions, which have huge implications of the microstructural parameters governing various physical properties.

II. EXPERIMENT

Single-phase $\text{LaNi}_x\text{V}_{1-x}\text{O}_3$ ($x = 0.0, 0.2, 0.4, 0.5, 0.8$, and 1.0) thin films were grown on (001)-oriented single-crystal LaAlO_3 (LAO) substrates using the pulsed laser deposition (PLD) technique. Fabrication of LVO film from single-phase polycrystalline LaVO_4 was described elsewhere [6]. To grow the $\text{LaNi}_x\text{V}_{1-x}\text{O}_3$ films, a number of dense pellets of each composition were used as a target for deposition. Bulk $\text{LaNi}_x\text{V}_{1-x}\text{O}_4$ were synthesized by a widely used solid-state reaction route. For the preparation of $\text{LaNi}_x\text{V}_{1-x}\text{O}_4$, proper amounts of highly pure (99.9%) La_2O_3 , V_2O_5 and NiO were mixed and annealed at 600°C for 6 h in air, followed by a second annealing at 1100°C for 20 h, with an intermediate grinding for 12 h. Lastly, the $\text{LaNi}_x\text{V}_{1-x}\text{O}_4$ targets were sintered at 1150°C for 15 h. It is important to mention here that as the La_2O_3 is a hygroscopic compound, it absorbs moisture over time and converts to lanthanum hydroxide. Thus, prior to the weighing, La_2O_3 was heated at 1050°C for 10 h to reduce the moisture effect. Then, precursors were weighed according to the required stoichiometry. Now we discuss the optimal deposition conditions employed in the present work using PLD for obtaining the stoichiometric single-phase $\text{LaNi}_x\text{V}_{1-x}\text{O}_3$ films. Deposition of $\text{LaNi}_x\text{V}_{1-x}\text{O}_3$ films was carried out using single-phase polycrystalline $\text{LaNi}_x\text{V}_{1-x}\text{O}_4$ target with a laser repetition rate of 3 Hz and a fluence of ≈ 1.8 to 2.0 J/cm^2 . The target to substrate distance was maintained at 5.0 cm during deposition. The substrate temperature was

kept at 650°C during deposition. To grow the $\text{LaNi}_x\text{V}_{1-x}\text{O}_3$ ($x = 0.0, 0.2, 0.4$, and 0.5) films, a vacuum near $\approx 5 \times 10^{-6}$ Torr was used, while for $\text{LaNi}_{0.8}\text{V}_{0.2}\text{O}_3$ film 70-mTorr oxygen partial pressure (OPP) was used, as optimized for obtaining its single phase. After deposition, the $\text{LaNi}_x\text{V}_{1-x}\text{O}_3$ films were cooled to the RT at the rate of 10°C/min in the same pressure as used during deposition. LNO film was deposited at OPP value of 350 mTorr and substrate temperature of 750°C . Post-deposition *in situ* annealing of the LNO film was carried out in oxygen at a pressure of 380 Torr for 1 h to avoid formation of oxygen vacancies and also maintain the phase stoichiometry of the film [31]. It is well known that the optimal growth condition in PLD allows us to capture a correct cation and anion stoichiometry.

In order to confirm the single-phase and stoichiometry nature of the grown films, we have performed x-ray diffraction (XRD) and energy-dispersive analysis of x-ray (EDAX) studies, respectively, after each deposition. The structural characterization of the grown films was done by a Bruker D2 Phaser x-ray diffractometer using $\text{Cu } K\alpha$ ($\lambda = 1.5406\text{ \AA}$) radiation. In-plane θ - 2θ XRD of the films was done by a PANalytical Empyrean high-resolution x-ray diffractometer. The composition of the grown films was verified by an EDAX unit attached with a field-emission scanning electron microscope (FEI NOVA Nano Sem 450) and found to be consistent with the nominal composition. Thickness of all the grown films were about 20 to 25 nm, as measured using the stylus profilometer. The x-ray photoemission spectroscopy (XPS) measurements of the grown films were carried out with Al $K\alpha$ (1486.6 eV) x-ray source using the Omicron energy analyzer (EA-125, Germany). RT valence-band spectra (VBS) of films were recorded at photon energy of 52 eV at the angle-integrated photoemission spectroscopy beamline on Indus-1 synchrotron source at Raja Ramanna Centre for Advanced Technology (RRCAT), Indore, India. The base pressure in the experimental chamber during measurements was on the order of 10^{-10} Torr. Prior to the photoemission measurements, the surface of all the films were cleaned *in situ* using low-energy Ar^+ ions. For calibration of binding energies, Au foil was kept in electrical contact with the sample and the Fermi level (E_F) was aligned using the VBS of Au foil. The total instrumental resolution was about 300 meV at $h\nu = 52\text{ eV}$. To investigate the unoccupied states of the grown films, x-ray absorption near-edge spectroscopy (XANES) was carried out at RT in the total electron yield mode at the beam line BL-01, Indus-2 synchrotron source at RRCAT, Indore, India. The energy resolution during XANES measurements across the measured energy range was estimated to be $\sim 250\text{ meV}$.

III. RESULTS AND DISCUSSION

A. Crystal structure

Figure 1(a) shows the RT θ - 2θ XRD patterns of $\text{LaNi}_x\text{V}_{1-x}\text{O}_3$ ($x = 0.0, 0.2, 0.4, 0.5, 0.8$, and 1.0) films along with single-crystalline LAO substrate. The diffraction pattern reveals the single-phase growth of all the films along the (00 l) direction. The calculated pseudocubic out-of-plane lattice parameter of grown LVO ($x = 0.0$) film is found to be 4.04 \AA .

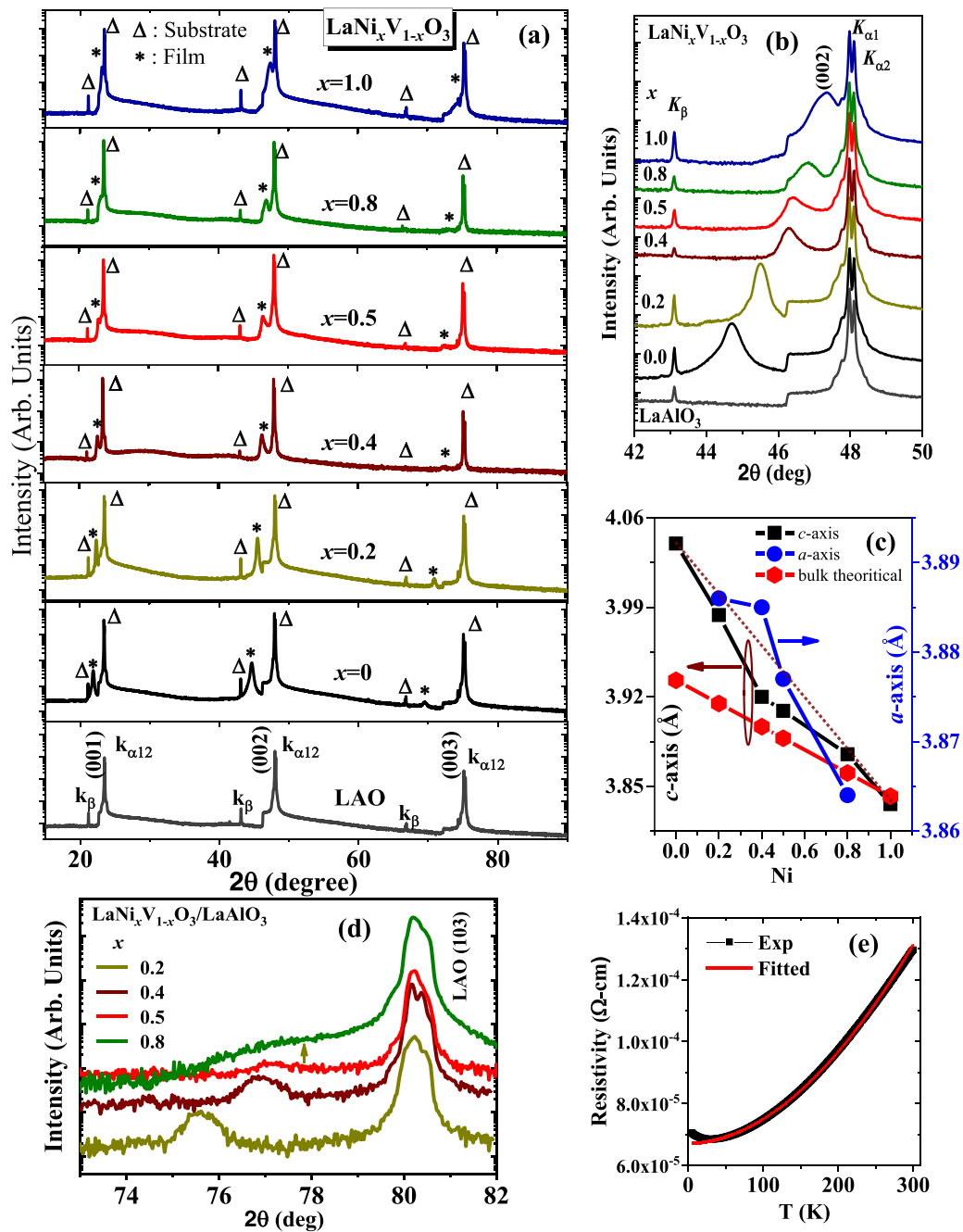


FIG. 1. (a) Room temperature θ - 2θ XRD patterns of $\text{LaNi}_x\text{V}_{1-x}\text{O}_3$ thin films grown on (001) LaAlO_3 substrates. (b) Zoomed view of the XRD pattern across the (002) peak. (c) Variation of calculated pseudocubic out-of-plane and in-plane lattice parameters with Ni doping in LVO films, along with expected pseudocubic bulk lattice parameters. (d) RT in-plane θ - 2θ XRD patterns of the $\text{LaNi}_x\text{V}_{1-x}\text{O}_3$ thin films across (103) plane. (e) Temperature-dependent resistivity of LaNiO_3 thin film grown on LaAlO_3 substrate.

The pseudocubic lattice parameter of bulk LVO is 3.93 Å [32]. The lattice mismatch with the underlying LAO substrate (lattice parameter of 3.79 Å) will induce in-plane compressive strain in the film, leading to the observed enhanced out-of-plane lattice parameter of LVO film with respect to its bulk counterpart. Zoomed view of the (002) peak, as shown in Fig 1(b), shows the systematic shift in the peak positions towards higher 2θ value with the increase in Ni concentration in LVO, suggesting the substitutional nature of Ni in the system. The shift in the peaks towards higher angle confirms that the out-of-plane lattice parameter of the grown films gradually

decreases, as shown in Fig. 1(c). As the Ni^{3+} has an ionic radius of 0.74 Å in an octahedron environment, whereas that of V^{3+} is 0.78 Å, a decrease in the lattice parameter and unit-cell volume is expected on increasing the Ni content in LVO. Thus, the average pseudocubic out-of-plane lattice parameter of $\text{LaNi}_x\text{V}_{1-x}\text{O}_3$ films is found to decrease from 3.98 Å in $\text{LaNi}_{0.2}\text{V}_{0.8}\text{O}_3$ to 3.88 Å in $\text{LaNi}_{0.8}\text{V}_{0.2}\text{O}_3$. The obtained out-of-plane lattice parameter 3.84 Å of LNO ($\text{LaNi}_x\text{V}_{1-x}\text{O}_3$, $x = 1.0$) film, which is slightly elongated compared to the pseudocubic bulk LNO (3.830 Å), is comparable to the previous results [31]. The grown films were epitaxial in nature

as confirmed from the in-plane phi scan of the (103) peak (not shown here). The in-plane lattice parameters of the $\text{LaNi}_x\text{V}_{1-x}\text{O}_3$ films were obtained from the (103) Bragg reflection of the grown film, using the formula $a = \sqrt{\frac{h^2 + k^2}{(\frac{1}{a^2} - \frac{l^2}{c^2})}}$ and plotted as a function of Ni concentration [Fig. 1(c)]. The systematic shifting of 2θ position of the (103) peak with Ni doping is shown in Fig. 1(d).

Usually the pseudocubic lattice constant of doped compounds is linearly dependent on doping level [33,34]. As the pseudocubic lattice parameter of bulk LNO is $a_p^{\text{LNO}} = 3.83 \text{ \AA}$ and bulk LVO is $a_p^{\text{LVO}} = 3.93 \text{ \AA}$, hence the pseudocubic lattice parameter for doped compounds $\text{LaNi}_x\text{V}_{1-x}\text{O}_3$ should vary linearly following the equation $a_p^{\text{LaNi}_x\text{V}_{1-x}\text{O}_3} = a_p^{\text{LNO}}(x) + a_p^{\text{LVO}}(1-x)$. However, as shown in Fig. 1(c), the obtained in-plane and out-of-plane lattice parameters of $\text{LaNi}_x\text{V}_{1-x}\text{O}_3$ films deviate from linearity as compared to the expected pseudocubic bulk $\text{LaNi}_x\text{V}_{1-x}\text{O}_3$. The deviation from the linearity arises because of the combined effect of chemical substitution and lattice misfit strain imposed by the underlying LAO substrate owing to the pseudomorphic growth of the films.

The temperature-dependent four-probe resistivity measurement of the LNO film shows the metallic behavior down to the low temperature and the electrical resistivity is obtained to be the order of $\sim 10^{-4} \Omega \text{ cm}$ at RT, which is similar to the previous reported value of the LaNiO_3 single crystal [35]. In order to find the residual resistivity (ρ_0) value of the present studied LNO film, we have further fitted the experimental data with the power law $\rho(T) = \rho_0 + AT^n$, as shown in Fig 1(d). We found that $\rho(T)$ could be fitted well with the power law with the value of $\rho_0 = 6.709 \times 10^{-5} \Omega \text{ cm}$, $A = 1.1846 \times 10^{-9} \Omega \text{ cm/K}^2$, and $n = 1.9$. Such lower ρ_0 value of the grown LNO film further confirms the good quality of the present studied film, although the residual resistivity is found to be slightly higher than previously reported for single-crystal ($13.9 \mu\Omega \text{ cm}$) and epitaxial thin film ($27.6 \mu\Omega \text{ cm}$) grown on SrTiO_3 (STO), which can be attributed to the presence of substrate-induced lattice misfit strain in the film that is higher on the LAO substrate as compared to the STO substrate [35,36].

B. Electronic structure

1. Core-level photoelectron spectrum

LNO is a paramagnetic metal, so Ni doping in LVO can facilitate electron delocalization. Such modification will also be manifested in the core-level spectra via final states of core-level photoemission. Figure 2(a) depicts the V $2p$ and O $1s$ core-level XPS of LVO and the intermediate compositional $\text{LaNi}_{0.5}\text{V}_{0.5}\text{O}_3$ films. The spectrum consists of spin-orbit split V $2p$ states along with O $1s$ state. To estimate the position of individual features of LVO, we have fitted the spectrum with a combination of Gaussian and Lorentzian functions and the background of the spectrum was corrected by the Shirley function as described elsewhere [6]. The obtained binding-energy (BE) position of the spin-orbit split V $2p_{3/2}$ and V $2p_{1/2}$ states for LVO are 515.6 and 522.8 eV, in conformity with the V^{3+} state in LVO bulk [37]. Similar BE positions of the V $2p_{3/2}$ and V $2p_{1/2}$ states are also observed for

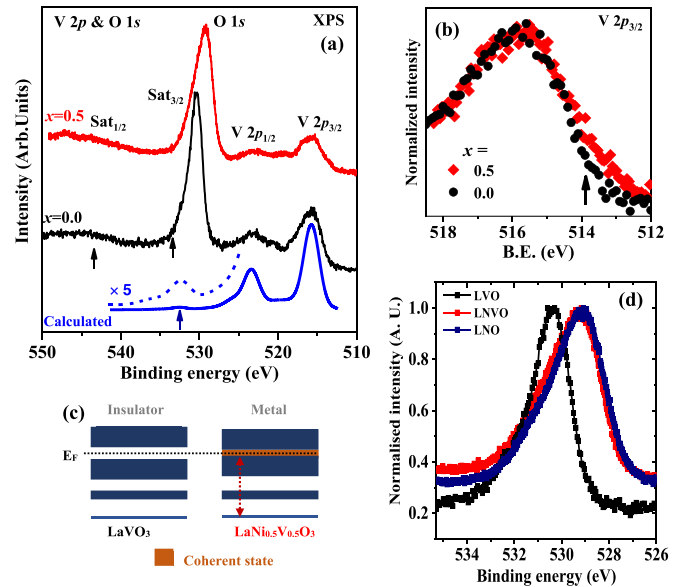


FIG. 2. (a) Experimental V $2p$ and O $1s$ XPS of $\text{LaNi}_x\text{V}_{1-x}\text{O}_3$ ($x = 0.0, 0.5$) thin films and simulated XPS of V^{3+} state at RT. (b) Zoomed view of the V $2p_{3/2}$ peak of $\text{LaNi}_x\text{V}_{1-x}\text{O}_3$ ($x = 0.0, 0.5$) thin films. (c) Schematic illustration of the emergence and absence of coherent state in metal and insulator. (d) O $1s$ core-level spectra of $\text{LaNi}_x\text{V}_{1-x}\text{O}_3$ ($x = 0.0, 0.5, 1.0$) thin films.

$\text{LaNi}_{0.5}\text{V}_{0.5}\text{O}_3$ film, confirming the formal charge state of V to remain in $3+$ after Ni doping in LVO. There is an overall broadening of spectral feature of V $2p$ on substituting Ni in LVO. Generally, the asymmetry and broadening in the V $2p$ photoelectron spectrum of V^{3+} state arise due to the occurrence of multiplet structure owing to the presence of unpaired electrons [38]. However, a slight enhanced broadening of V $2p$ photoelectron spectrum is evident in $\text{LaNi}_{0.5}\text{V}_{0.5}\text{O}_3$, in the form of an appearance of a shoulder structure at lower BE to the main V $2p_{3/2}$ peak as shown clearly in Fig. 2(b). A similar behavior was reported in the V $2p$ photoelectron spectra of V_2O_3 and VO_2 observed across the MIT [39,40]. It has been suggested that such low-BE shoulder structure in V $2p_{3/2}$ peak of V_2O_3 and VO_2 arises due to the extra screening of V $2p$ electrons from coherent states, created at the E_F upon insulator to metal transition. Moreover, the configuration-interaction cluster-model analysis confirms that inclusion of an extra charge transfer from the coherent band to the upper Hubbard band, defined as the energy difference between the configuration-averaged energies $E(3d^3\bar{C}) - E(3d^2)$, where \bar{C} represents the hole in the coherent states just below E_F , describes the low-BE structure in the metallic phase [41]. Therefore, the observed shoulder structure at lower BE to the main V $2p_{3/2}$ peak of $\text{LaNi}_{0.5}\text{V}_{0.5}\text{O}_3$ film confirms the emergence of the coherent states with Ni doping in LVO as shown schematically in Fig. 2(c). The O $1s$ core-level photoelectron spectra also show a clear spectral shape change, a narrow symmetric peak in insulating LVO to a broad asymmetric line shape in $\text{LaNi}_{0.5}\text{V}_{0.5}\text{O}_3$ and LNO as shown in Fig. 2(d). The asymmetry in line shape of the core-level photoelectron spectrum arises due to the electron-hole pair shake-up excitation, directly related to the metallic screening [42]. The asymmetric

to symmetric line shape changes are similar to those observed in the O 1s spectra of V_2O_3 and VO_2 across MIT and metallic $SrVO_3$, $CaVO_3$ compounds [43]. Thus, a change in line shape of O 1s spectrum in $LaNi_{0.5}V_{0.5}O_3$ film indicates the creation of coherent states at E_F , a signature of metallic nature of $LaNi_{0.5}V_{0.5}O_3$ film.

We have further simulated the V 2p core-level spectrum using the charge transfer multiplet calculation [44], which very much represents the experimental spectrum as shown in Fig. 2(a). As the core-level spectrum was recorded using the x-ray source, thus the simulated spectrum was further convoluted with a 0.7-eV Gaussian to account for the instrumental resolution. Apart from the sharp V $2p_{3/2}$ and V $2p_{1/2}$ main peaks at 515.6 and 523.4 eV, a weak intense satellite structure is also observed around 532.5-eV BE position. The cluster-model calculation on LVO suggests that the main peaks V $2p_{3/2}$ and V $2p_{1/2}$ states correspond to the well-screened $c3d^3\bar{L}$ (c : hole in the core level, \bar{L} : hole in O 2p band) final-state configuration, whereas the CT satellite structure corresponds to the poorly screened $c3d^2$ configurations and appears at the higher BE side of the O 1s peak (~ 532 eV) and around 542 eV, respectively [43]. As the satellite structure of V $2p_{3/2}$ state appears at 532.5 eV and is buried in the higher BE side of the O 1s peak, it causes a slight asymmetric shape of O 1s even in insulating LVO.

2. Near-edge x-ray absorption spectroscopy

To understand the modifications in local electronic structure of Ni-doped LVO films, we performed the near-edge x-ray absorption spectroscopy (NEXAS) of $LaNi_xV_{1-x}O_3$ films. Figure 3(a) shows the V $L_{3,2}$ -edge absorption spectra of the $LaNi_xV_{1-x}O_3$ films measured at RT. The corresponding V L -edge spectra are further compared with the spectrum of trivalent V_2O_3 (V^{3+} : $3d^2$) and pentavalent V_2O_5 (V^{5+} : $3d^0$) compounds. The energy position of the absorption maxima of L_3 edge of $LaNi_xV_{1-x}O_3$ films is similar to those of V_2O_3 but quite different from those of V_2O_5 and VO_2 [45], which confirms that V ions are formally in trivalent (V^{3+} : $3d^2$) state in the present studied $LaNi_xV_{1-x}O_3$ films. The maxima of V $L_{3,2}$ absorption peaks of the $LaNi_xV_{1-x}O_3$ films appear at the position of 517.8 and 523.8 eV, in conformity with the previous XAS measurements of single crystal and thin film of LVO and other RVO_3 compounds [6,46,47]. However, substantial change is observed in the line shape of the L_3 absorption peak. As the doping of Ni increases, the full width at half maximum of the V L_3 peak decreases, resulting in the narrowing of the L_3 peak and concomitantly the more pronounced low-energy shoulder is observed with increasing x in $LaNi_xV_{1-x}O_3$ films. This trend is shown more clearly at the top of Fig. 3(c), where two XAS of $x = 0.8$ ($LaNi_{0.8}V_{0.2}O_3$) and $x = 0$ ($LaVO_3$) are normalized at the maximum intensity. Interestingly, this shoulder structure shifts towards lower energy with increasing Ni concentration in LVO. Such enhancement of shoulder structure was also observed in Mn L_3 edge of $SrMn_{1-x}Fe_xO_3$ with increase in x [48] and was attributed to the charge transfer effect between the Mn 3d and O 2p orbitals. Generally, the line shape of the V $L_{3,2}$ absorption peaks depends on the atomic multiplet states, crystal field, and ligand to metal CT effect [49]. The crystal-field splitting is caused by the interac-

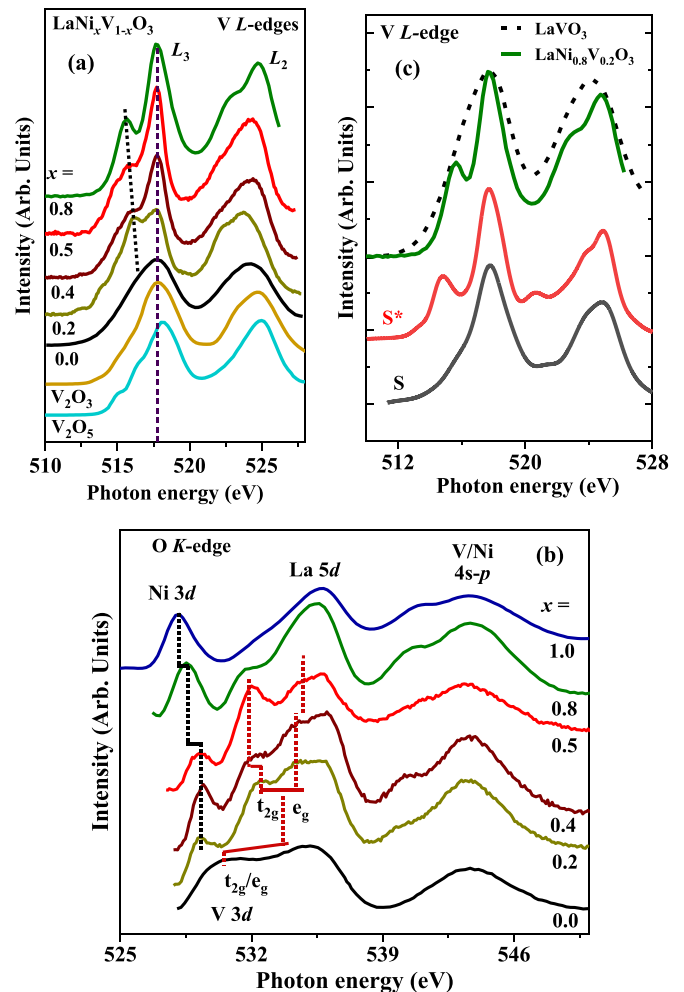


FIG. 3. (a) RT V 2p NEXAS of $LaNi_xV_{1-x}O_3$ thin films along with trivalent V_2O_3 and pentavalent V_2O_5 compounds. (b) O 1s NEXAS of $LaNi_xV_{1-x}O_3$ thin films at RT. (c) Experimental and simulated V^{3+} L -edge spectra of $LaVO_3$ and $LaNi_{0.8}V_{0.2}O_3$ thin films at RT.

tion of metal d electrons with the surroundings ligand ions in the crystals, whereas the multiplet states are originated due to the intra-atomic $3d$ - $3d$ Coulomb and $2p$ - $3d$ Coulomb and exchange interactions [49]. Moreover, these effects enormously depend on the local site geometry in a crystal, such as M -O- M networks and the corresponding hybridization between metal $3d$ and oxygen $2p$ ions [50]. Thus, the more pronounced shoulder structure of the V L_3 peak and its shifting towards lower energy with increasing Ni doping in LVO imply the modulation in local structural symmetry and corresponding energetics. To understand the mechanism behind the emergence of prepeak structure in V L_3 edge with Ni doping, we have further simulated the V^{3+} L edge using charge transfer multiplet calculation [44].

Figure 3(b) shows the O K -edge NEXAS of all $LaNi_xV_{1-x}O_3$ films. The O K -edge spectrum corresponds to the transition of an electron from the O 1s core-level to the unoccupied O 2p states hybridized with the metal 3d and rare-earth 5d states [51]. For LVO (V^{3+} : $3d^2$), the lower-energy structure in the photon energy range of 529.0 to 532.5 eV

primarily corresponds to the O $2p$ character mixed with the unoccupied part of the V $3d$ state, whereas other broad structures appearing around 535.0 and 540–545 eV are due to the O $2p$ character mixed with the La $5d$ and V $4s-4p$ hybridized states [6] as shown in Fig. 3(b). In LVO, perovskite cubic octahedral (O_h) symmetry splits the V $3d$ levels into threefold t_{2g} and twofold e_g levels. Thus, the broad feature appearing in the photon energy range of 529.0 to 532.5 eV is attributed to the hybridized O $2p$ -V t_{2g} and e_g states, respectively. With respect to the thicker and single-crystal LVO studies, in the studied thin film of LVO these peaks appear closer and form a broad structure, revealing lesser effective crystal-field energy (Δ_{CF}) (~ 1 eV) than 1.3 and 1.8 eV obtained for thicker and single-crystal LVO, respectively [6,43]. Such reduction in Δ_{CF} value in the studied LVO film possibly arises due to the alteration of local symmetry from O_h in bulk/thick film to D_{4h} in thinner film, which leads to the asymmetric variation in V–O bond length (reduction in the in plane and expansion along out of plane), and hence affecting the Δ_{CF} , as $\Delta_{CF} \propto (V-O)^{-5}$ [52].

In $\text{LaNi}_x\text{V}_{1-x}\text{O}_3$ ($x = 0.2, 0.4, 0.5, 0.8,$ and 1.0) films, a sharp feature appears at the photon energy of 529.2 eV and remains fixed in energy up to 50% Ni substitution in LVO as shown in Fig. 3(b). Interestingly, this feature shifts further towards lower photon energy with the enhanced Ni concentration and finally appears at 528.2 eV for LNO ($x = 1.0$) similar to previous reports [53,54]. This peak is attributed to the unoccupied Ni $3d$ states, mostly dominated by e_g character. In rare-earth nickelates, due to the strong Ni $3d$ -O $2p$ hybridization, the ground state is composed of a mixture of configuration $3d^7, 3d^8\bar{L}, 3d^9\bar{L}^2$ (\bar{L} : ligand hole), instead of purely ionic configuration ($\text{Ni}^{3+}\text{O}^{2-}$). Resultantly, the ground state has an appreciable amount of $3d^8\bar{L}$ character that causes such preedge structure, which is attributed to the transition $3d^8\bar{L} \rightarrow \bar{c}3d^8$ (\bar{c} : O $1s$ core-hole) [55] and is treated as a mark of Ni $3d$ -O $2p$ hybridization strength. It is important to mention here that with reduced Ni concentration, obtained preedge feature in O K edge of $\text{LaNi}_x\text{V}_{1-x}\text{O}_3$ films is shifted towards higher photon energy by around 1.0 eV as compared to LNO (Ni^{3+}) film. Earlier, the movement of such prepeak towards higher energy was reported to occur in epitaxial LNO films with enhanced substrate-induced strain [19] and was ascribed to the reduced Ni–O bond covalency and corresponding enhancement of charge transfer energy (Δ) [56]. Therefore, such shifting of prepeak towards higher energy in the present studied $\text{LaNi}_x\text{V}_{1-x}\text{O}_3$ films could be explained in terms of the reduced covalency of Ni, as expected from the enhanced Ni–O distances with reduction in Ni concentration in LVO. Similar correlation between Cu–O distance and the energy threshold of the prepeak has been drawn for the insulating precursors of several high- T_C superconductors [57]. Similar prepeak was also present in O $1s$ XAS of NiO (Ni^{2+}) corresponding to $3d^9\bar{L} \rightarrow \bar{c}3d^9$ transition [54]; however, its energy position (532.0 eV) is about 3.0 eV higher than the prepeak of $\text{LaNi}_{0.2}\text{V}_{0.8}\text{O}_3$ film that invalidates the presence of Ni^{2+} in the present studied $\text{LaNi}_x\text{V}_{1-x}\text{O}_3$ films. Furthermore, splitting in this prepeak was observed in the oxygen-deficient LNO compounds as shown in a study by Abbate *et al.* [55]. Based on cluster-model calculation, splitting has been attributed to the presence of two nonequivalent crystallographic sites owing to

the oxygen deficiency. However, no such splitting has been observed in the prepeak of presently studied $\text{LaNi}_x\text{V}_{1-x}\text{O}_3$ films, which further rules out the presence of oxygen defect states.

Importantly, Ni doping in LVO leads to the substantial modification in the energy position of unoccupied V $3d$ state as shown in Fig. 3(b). A peak observed at 532.4 eV in the O K edge of $\text{LaNi}_{0.2}\text{V}_{0.8}\text{O}_3$ film, which is absent in LNO film, represents the unoccupied V $3d$ states. It appears that with Ni doping in LVO films, a spectral feature representing the Ni $3d$ -O $2p$ hybridization emerges at lower photon-energy side of the unoccupied V $3d$ band, which subsequently pushes the V $3d$ band towards higher energy. Moreover, the V t_{2g} and e_g states, which are merged together and form a broad structure in LVO, appear to be separated with two isolated relatively narrow features in Ni-doped LVO films as shown in Fig. 3(b). It is observed that even with the doping of 20 at. % Ni, the local strain is relieved, transforming the symmetry from D_{4h} to O_h and hence well-separated crystal-field split t_{2g} and e_g states for V $3d$ states are observed. Such changes in local strain can be realized also from the sharp change in the lattice parameter c and its deviation from the linearity. Furthermore, as the Ni concentration increases, the separation between the V t_{2g} and e_g states increases, suggesting an increase in the crystal-field splitting owing to the combined effect of lattice misfit strain and Ni substitution in LVO. The spectral feature at 535.4 eV and broad structures appearing around 540–545 eV for all the $\text{LaNi}_x\text{V}_{1-x}\text{O}_3$ films correspond to the unoccupied La $5d$ and Ni/V $4s-4p$ hybridized states [53].

In the V L -edge spectra, it should be noted that on going from LaVO_3 to $\text{LaNi}_{0.8}\text{V}_{0.2}\text{O}_3$, the V $L_{3,2}$ absorption peak narrows and shoulder or prepeak feature is enhanced. To better understand this trend, we compare the V $2p$ XAS spectra of LaVO_3 ($x = 0$) and $\text{LaNi}_{0.8}\text{V}_{0.2}\text{O}_3$ ($x = 0.8$) with those of simulated V^{3+} L -edge spectrum using charge transfer multiplet program for x-ray absorption spectroscopy (CTM4XAS) [44] as shown in Fig. 3(c). The shape of V L_3 and L_2 lines is very sensitive to the Δ_{CF} along with the V^{3+} ground-state ($2p^6 3d^2$) and excited-state ($2p^5 3d^3$) multiplets, which can be controlled by the two-particle interaction parameter. Therefore, we performed calculations by varying the reduction of Slater integrals, the crystal-field splitting (Δ_{CF}), charge transfer energy (Δ), d - d interaction energy (U), and O $2p$ -V $3d$ hybridization strength. Slater integrals were reduced to 70% of their atomic values to simulate both spectra. The simulated $L_{3,2}$ -edge spectrum of V^{3+} with d^2 (3T_1) ground state along with the crystal field in O_h symmetry of 1.0 eV, $\Delta = 6.8$ eV, $U_{2p3d} - U_{3d3d} = 2.2$ eV, and hopping parameter $V(e_g) = 2.8$ eV matches well with the experimentally observed V L -edge spectrum of LaVO_3 [marked as feature S in Fig. 3(c)]. The simulated line spectrum is convoluted with Lorentzian line shape equal to the lifetime width 0.4 eV of the L_3 core-hole and with a Gaussian linewidth 0.25 eV to represent instrumental broadening. Although both the simulated profiles agree well with the experimental profiles of V L edge, the minor source of discrepancy could be due to the nonuniformity of the core-hole lifetime broadening. To understand the modifications in V L -edge spectrum with Ni doping, we further alter the different parameters to simulate the V^{3+} L -edge spectrum for $\text{LaNi}_{0.8}\text{V}_{0.2}\text{O}_3$ film. It is ob-

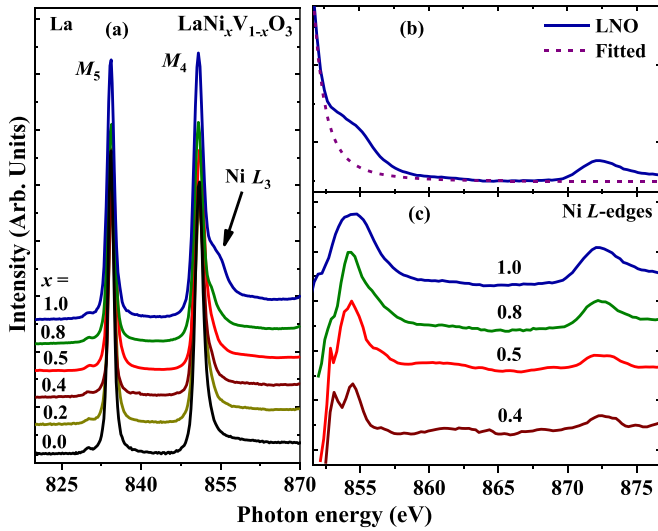


FIG. 4. (a) La $M_{5,4}$ - and Ni L_3 -edge spectra of $\text{LaNi}_x\text{V}_{1-x}\text{O}_3$ thin films at 300 K. (b) For the Ni L -edge spectrum of LNO films, the La $3d_{3/2}$ absorption peak (indicated by dashed line) was subtracted from raw data. (c) Extracted Ni $L_{3,2}$ -edge spectra of $\text{LaNi}_x\text{V}_{1-x}\text{O}_3$ films [For extraction of Ni L edge of Ni-doped LVO films the same procedure has been followed as mentioned in (b)].

served that with higher $\Delta_{\text{CF}} = 2.4$ eV and lower Δ value (~ 3.0 eV), a quite intense prepeak generated. It is known that the crystal-field interaction mixes states with different L values in the ground state such that the transition to other final states is allowed with the same spin [58]. Such mixing gives rise to the broadening of the peaks and a gradual appearance of new peaks with increasing crystal fields. Our observed intense prepeak in $\text{LaNi}_{0.8}\text{V}_{0.2}\text{O}_3$ film and well-simulated V^{3+} L -edge spectrum marked as S^* in Fig. 3(c) with considering higher Δ_{CF} and lower Δ compared to LVO film suggests an increase in metal-ligand hybridization with Ni doping in LVO. The enhanced Δ_{CF} in $\text{LaNi}_x\text{V}_{1-x}\text{O}_3$ films with higher x values is further confirmed in O K -edge oxygen spectra of Ni-doped films. Previously enhanced charge transfer energy or weaker covalency [48] was suggested to be the primary cause for the broadening of $L_{3,2}$ absorption peaks; however, our observation from simulation suggests that peak broadening is very much sensitive to the variation of Δ_{CF} .

Figure 4(a) shows the La $M_{5,4}$ - and Ni L_3 -edge spectra of $\text{LaNi}_x\text{V}_{1-x}\text{O}_3$ films measured at 300 K. The La $M_{5,4}$ -absorption peaks arise due to transition of an electron from spin-orbit split La $3d$ core level to the unoccupied La $4f$ states. Observed energy positions of La $M_{5,4}$ edge for all the films match well with that of La^{3+} reported in literature [59], confirming the $3+$ charge state of La. Owing to very small energy separation between La $3d_{3/2}$ and Ni $2p_{3/2}$ core levels, the La M_4 - and Ni L_3 edges overlap as shown in Fig. 4(a) [60]. Hence, in order to study the Ni L -edge spectra, it was extracted by fitting multiple Lorentzian peaks to the overlapped region and then subtracting La M_4 edge from raw data as shown in Fig. 4(b) [61]. The extracted Ni $L_{3,2}$ -edge spectra of $\text{LaNi}_x\text{V}_{1-x}\text{O}_3$ films are shown in Fig. 4(c). Interestingly, like V L edge, the Ni L edge also shows drastic variation with increasing Ni concentration in LVO. The observed L_3

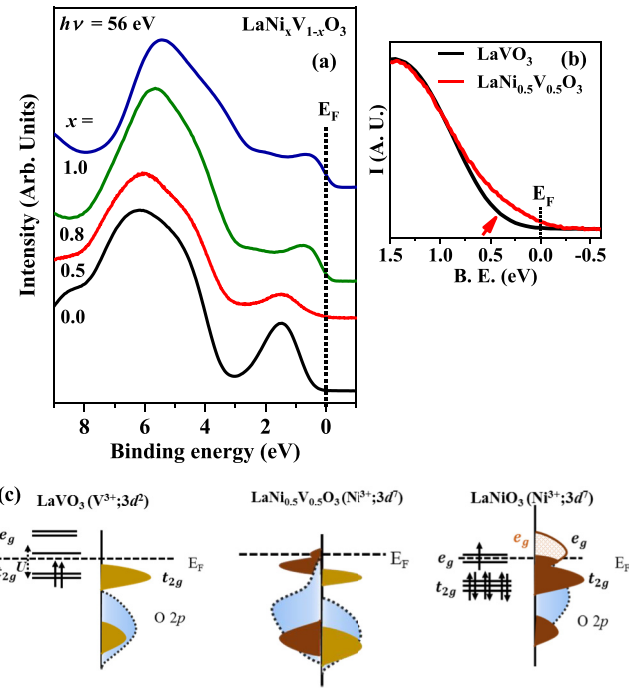


FIG. 5. (a) RT VBS of $\text{LaNi}_x\text{V}_{1-x}\text{O}_3$ thin films recorded at 56-eV incident photon energy. (b) Zoomed view of VBS of LaVO_3 and $\text{LaNi}_{0.5}\text{V}_{0.5}\text{O}_3$ thin films near E_F . (c) Schematic representation of V $3d$, Ni $3d$, and O $2p$ bands in valence band obtained from the VBS of $\text{LaNi}_x\text{V}_{1-x}\text{O}_3$ thin films.

edge for higher Ni concentrated $\text{LaNi}_{0.8}\text{V}_{0.2}\text{O}_3$ and LNO films show a single-peak structure, while lower Ni concentrated $\text{LaNi}_{0.5}\text{V}_{0.5}\text{O}_3$, $\text{LaNi}_{0.4}\text{V}_{0.6}\text{O}_3$ films show double-peak structure. Moreover, the L_3 -edge line shape of $\text{LaNi}_{0.8}\text{V}_{0.2}\text{O}_3$ film is much narrower compared to the LNO film. The Ni L -edge spectrum of nickelates exhibits distinct double-peak structures originating from $2p^6 3d^8 - 2p^5 3d^9$ and $2p^6 3d^8 L^n - 2p^5 3d^9 L^n$ multiplet transitions [54]. However, the relative intensity and the separation between the double peak depends on the energetic balance among microscopic parameters, including site energy, charge transfer energy, and rare-earth Ni hybridization energy, which are expected to vary in $\text{LaNi}_x\text{V}_{1-x}\text{O}_3$ films [54]. The energy position of Ni L_3 edge confirms the Ni^{3+} valence state in Ni-doped LVO films. The trivalent valence states for both V and Ni ions in $\text{LaNi}_x\text{V}_{1-x}\text{O}_3$ films suggest that Ni doping in LVO does not lead to the carrier doping in the valence band of LVO, rather the modification in bandwidth due to alteration in TM-oxygen hybridization upon Ni doping.

3. Valence-band spectra

The VBS of $\text{LaNi}_x\text{V}_{1-x}\text{O}_3$ ($x = 0.0, 0.5, 0.8$, and 1.0) films are recorded at photon energy of 56 eV at 300 K is shown in Fig. 5(a). It has been shown previously [6,62] that for LVO, the spectrum in the BE range between 0.5 eV and 3.0 eV is due to the dominant V $3d$ character, and the energy region between 3.0 and 9.0 eV is mostly dominated by the O $2p$ contribution. The resonant photoemission spectroscopy (RPES) study of LVO film at 300 K [6] further confirmed the dominated V $3d$ states with $3d^{n-1}$ final-state character of the spectral feature centered at 1.5 eV and attributed to lower Hubbard

band (LHB), while the feature around 6.9 eV represented V $3d$ -O $2p$ hybridized band with $3d^n L$ final-state character schematically shown in Fig. 5(c). These observations are also corroborated with the theoretically calculated density of states (DOS) [13]. For LNO, previous studies suggest that BE region 7.5 to 3.5 eV is attributed to the O $2p$ bonding states and the region between 3.5 and 1.5 eV is assigned to the O $2p$ nonbonding states, while the spectrum from 1.5 to E_F corresponds to the Ni $3d$ states [54]. RPES study of $\text{LaNiO}_{3-\delta}$ thin films also suggests that the features near E_F have dominant Ni $3d$ band [63]; however, substantial amount of O $2p$ states in the form of hybridization are also present. The features at about 6.0 eV are due to the admixture of La $4d$ and O $2p$ states. Considering the electron configuration $t_{2g}^6 e_g^1$ for Ni^{3+} in LNO, it appears that the weak intense feature at E_F is related to the e_g band, while the feature at 1.0 eV is associated with the t_{2g} band [18], schematically shown in Fig. 5(c). The presence (absence) of finite spectral DOS at the E_F confirms the metallic (insulating) nature of LNO (LVO) film. The overall spectral features of VB of $\text{LaNi}_{0.5}\text{V}_{0.5}\text{O}_3$ film [Fig. 5(a)] appear somewhat similar to the VB of LVO; however, strong modification is observed at around 1.5 eV BE near the E_F , which turned out to be more asymmetric after Ni doping. To understand more on this aspect, we further normalized the spectra of $\text{LaNi}_{0.5}\text{V}_{0.5}\text{O}_3$ and LVO film at 1.5 eV, as shown in Fig. 5(b). Beside intense 1.5-eV feature, an additional shoulder structure appears at 0.3 eV in $\text{LaNi}_{0.5}\text{V}_{0.5}\text{O}_3$ film and the tail of this shoulder structure crosses the E_F , resulting in an enhancement of spectral DOS at E_F of $\text{LaNi}_{0.5}\text{V}_{0.5}\text{O}_3$. Such spectral enhancement at E_F represents the coherent states, which emerges due to the delocalized conduction electrons in $\text{LaNi}_{0.5}\text{V}_{0.5}\text{O}_3$ film. Such spectral DOS at E_F further enhances with the Ni doping in LVO as seen in the VBS of $\text{LaNi}_{0.8}\text{V}_{0.2}\text{O}_3$ film. In LNO, the spectral feature at the E_F is strongly dominated by the occupied Ni $3d$ states hybridized with O $2p$ bands. Thus, the observed shoulder feature near across E_F of $\text{LaNi}_x\text{V}_{1-x}\text{O}_3$ ($x = 0.5$ and 0.8) films is possibly due to the presence of the occupied Ni $3d$ states, schematically shown in Fig. 5(c), which provides delocalized electrons responsible for metallic conduction in the system.

To further understand the atomic origin of the spectral features, primarily near E_F in VBS of $\text{LaNi}_x\text{V}_{1-x}\text{O}_3$ films, we performed the V $3p \rightarrow 3d$ RPES of $\text{LaNi}_{0.5}\text{V}_{0.5}\text{O}_3$ film at 300 K and compared with LVO film. The on- and off-resonance spectra are recorded at the incident radiation of 52 and 40 eV, respectively, as shown in Fig. 6(a). Comprehensive study on the RPES of LVO film at 300 K is described elsewhere [6]. The difference spectrum, obtained by subtracting the off-resonance spectrum and inelastic background from the on-resonance spectrum, represents roughly the partial spectral weight distribution of the V $3d$ electrons. So, we consider this difference spectrum as V $3d$ spectral DOS of LVO film. It is important to note that the extracted V $3d$ spectral DOS of LVO film matches well with the calculated V $3d$ partial DOS (PDOS) of strained orthorhombic LVO obtained from the density-functional theory (DFT) using generalized gradient approximation for exchange correlation as shown in Fig. 6(c) [13]. It is evident for $\text{LaNi}_{0.5}\text{V}_{0.5}\text{O}_3$ film, shown in Fig. 6(b), that the spectral feature at 1.5 eV is strongly enhanced with V $3p \rightarrow 3d$ excitation threshold akin to the LVO film, indi-

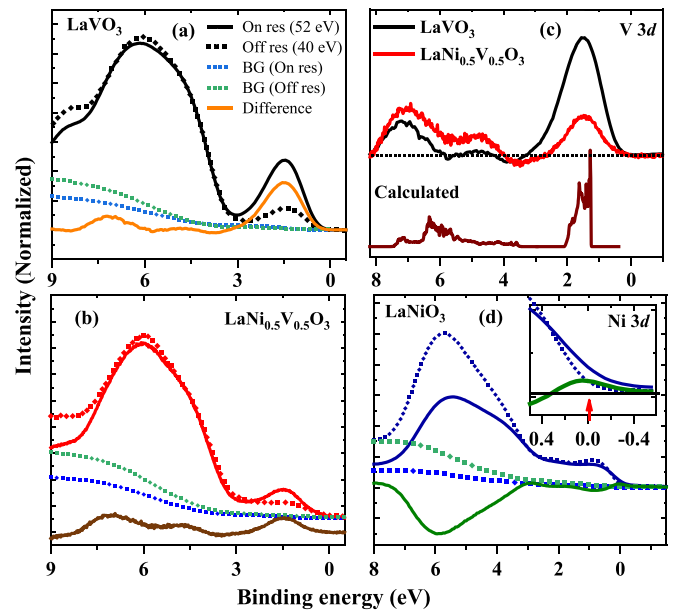


FIG. 6. (a) Extraction procedure of V $3d$ spectral DOS of LVO film at RT. The dotted line labeled as “BG” represents the rough estimation of inelastic background. See the text for details. (b) Extraction procedure of V $3d$ spectral DOS of $\text{LaNi}_{0.5}\text{V}_{0.5}\text{O}_3$ film at RT. (c) Comparison of the extracted V $3d$ spectral DOS along with calculated V $3d$ PDOS of strained orthorhombic LVO. (d) Extraction procedure of Ni $3d$ spectral DOS of LNO film at RT. (Inset) Zoomed view of the difference spectra near E_F .

cating that the feature at 1.5 eV has strong V $3d$ character. We have followed the same extraction procedure as described above to determine the V $3d$ spectral DOS of $\text{LaNi}_{0.5}\text{V}_{0.5}\text{O}_3$ film. Figure 6(c) shows the extracted V $3d$ spectral DOS of LVO and $\text{LaNi}_{0.5}\text{V}_{0.5}\text{O}_3$ films. It is found that V $3d$ spectral DOS exhibits a double-peak structure centered at 1.5 eV and around 6.9 eV BE, respectively, for both LVO and $\text{LaNi}_{0.5}\text{V}_{0.5}\text{O}_3$ films. The sharp peak appears at ~ 1.5 eV below E_F in the V $3d$ spectral DOS of LVO and $\text{LaNi}_{0.5}\text{V}_{0.5}\text{O}_3$ films, and is attributed to the dominant V t_{2g} band [6,62], whereas, the broad feature around 6.0–7.0 eV BE in V $3d$ spectral DOS represents the O $2p$ -V $3d$ hybridized states [6,62,13]. Interestingly, the V $3d$ spectral DOS around the O $2p$ -V $3d$ hybridized region appears extended in $\text{LaNi}_{0.5}\text{V}_{0.5}\text{O}_3$ compared to the LVO film, indicating increase in V $3d$ -O $2p$ hybridization with Ni doping in LVO film. Moreover, the spectral intensity ratio $I(1.5\text{ eV})/I(6.9\text{ eV})$ decreases, suggesting a transfer of V $3d$ spectral weight from localized incoherent state to V $3d$ -O $2p$ hybridized state with Ni doping in LVO as evident in Fig. 6(c). It is important to highlight here that the extracted V $3d$ spectral DOS of $\text{LaNi}_{0.5}\text{V}_{0.5}\text{O}_3$ film does not display spectral intensity at E_F [$I(E_F)$], which suggests that V $3d$ electrons are strongly localized even with Ni doping in LVO. So, the shoulder feature appearing near E_F of the VB of $\text{LaNi}_{0.5}\text{V}_{0.5}\text{O}_3$ film, which is also responsible for finite spectral DOS at E_F , could be attributed to the Ni $3d$ states. To confirm this we have also recorded the VBS of LNO film at on- and off resonance with incident radiation of 64 and 40 eV, respectively, shown in Fig. 6(d). Difference spectrum represents the spectral weight distribution of Ni $3d$ electron,

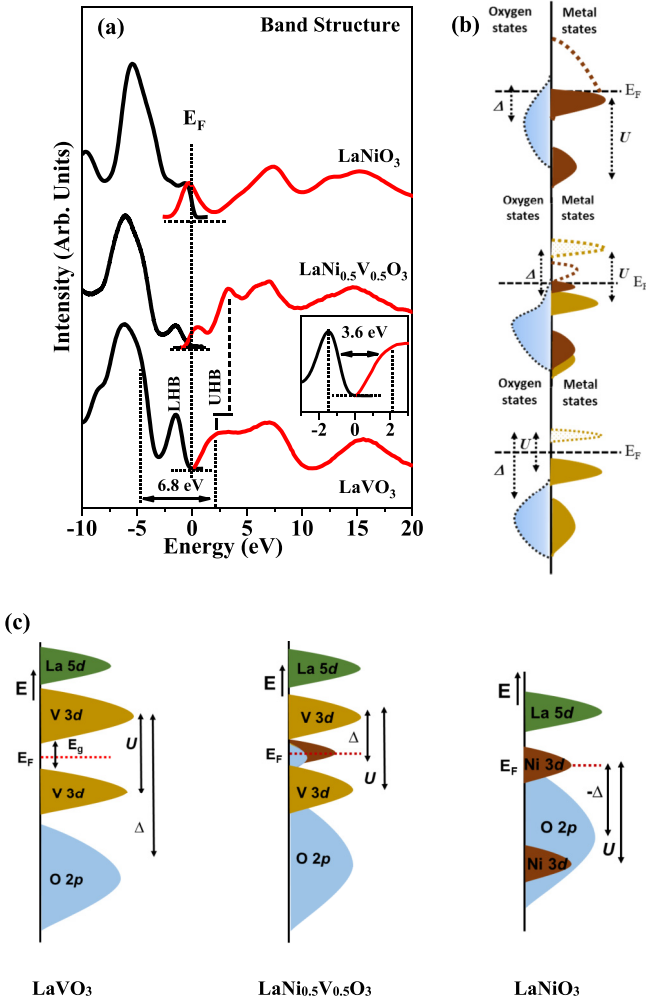


FIG. 7. (a) Combined valence and conduction bands of $\text{LaNi}_x\text{V}_{1-x}\text{O}_3$ thin films at RT. (Inset) Zoomed view of the band-edge portion of combined spectra of LVO film. (b) Schematic illustration of metal V and Ni 3d bands and oxygen 2p bands along with corresponding charge transfer (Δ) and Coulomb correlation (U) energies. (c) Schematics of the overall band structure as derived from these experimental observations.

which reveals a finite Ni 3d contribution near E_F , as clearly shown in the inset of Fig. 6(d). Thus, the shoulder feature in $\text{LaNi}_{0.5}\text{V}_{0.5}\text{O}_3$ confirms that the delocalized Ni 3d electrons are responsible for the metallic conduction in this system akin to the LNO [54,18]. Therefore, in $\text{LaNi}_x\text{V}_{1-x}\text{O}_3$ films, besides the presence of incoherent structure which represents the localized V 3d band, a coherent structure also appears which represents the Ni 3d band near and at E_F .

4. Electronic band structure across the Fermi level (E_F)

To understand the modulation of low-energy charge fluctuation across the E_F and the evolution of electronic states near E_F with the Ni substitution in LVO, the experimental VB and conduction band (CB) of $\text{LaNi}_x\text{V}_{1-x}\text{O}_3$ ($x = 0.0, 0.5, \text{ and } 1.0$) films are combined together, as shown in Fig. 7(a). For the CB, oxygen K -edge spectrum has been used, as it can be considered to represent the most weighted unoccupied character of

TM 3d, TM 4sp, and La 5d states via the hybridization with O 2p states. In addition, the photo induced core-hole effect on the final state DOS is less severe compared to the TM 2p edge [51]. To plot the CB, oxygen K edge of the $\text{LaNi}_x\text{V}_{1-x}\text{O}_3$ films was subtracted from the BE position of the rising tail of the oxygen core-level photoelectron spectrum [64,65]. Although O K -edge XAS has been used for the CB mapping, it does not reflect the true DOS of the transition-metal states, rather reflecting the oxygen 2p projected metal 3d DOS. The electronic structure of $\text{LaNi}_x\text{V}_{1-x}\text{O}_{3+x}$ films obtained from the experimental occupied and unoccupied DOS indicates a substantial modification in spectral DOS, mostly appearing near across the E_F with Ni doping in LVO film. In LVO film, as shown in Fig. 7(a), the first spectral feature in the VB appearing at -1.5 eV below the E_F has the dominant occupied V 3d character as confirmed through the RPES study [6] and DFT calculation [13]. Thus, this structure, normally termed as an incoherent feature in one-electron removal spectrum, is ascribed as a spectral signature of the LHB [6,62]. In the CB, the first prominent broad structure is observed from $+2.1$ to $+3.0$ eV above the E_F . The DFT calculation and the bremsstrahlung isochromat (BI) spectroscopic measurements on bulk LVO [13,62] confirmed that such spectral structure appeared due to the unoccupied V 3d t_{2g} and e_g structure. Hence, the unoccupied V t_{2g} state appearing at $\sim +2.1$ eV above E_F is attributed to the spectral signature of upper Hubbard band (UHB). The energy separation between the LHB and UHB was found to be ~ 3.6 eV, which is the energy difference between the d^{n-1} and d^{n+1} electronic state and related to the electron correlation strength (U) of the LVO film, clearly shown in the inset of Fig. 7(a). Such high electron correlation energy compared to the kinetic energy (bandwidth) of the LVO at 300 K impedes the electron delocalization; resultantly, an insulating state is emerged through electron localization at their lattice site even in partially occupied V t_{2g}^2 system [4,5]. The calculated band gap is about 1.0 eV as obtained from the combined spectra. The detailed analysis of the VBS described elsewhere [6] confirms that the O 2p band lies well below the V 3d band in LVO film, as schematically shown in Fig. 7(b), divulging the Mott-Hubbard type insulating nature of LVO film at RT [6].

Combined spectra show a large spectral DOS at the E_F of LNO film confirming its metallic nature at RT shown in Fig. 7(a) [54]. The VBS of LNO mimics the band structure of a negative charge transfer metal ($-\Delta$), as has been predicted earlier [66,67]. In these negative Δ materials, the band gap does not belong to either a p - d type or a d - d type; rather, it is a p - p type and the charge fluctuations can be viewed as $d^{n+1}\underline{L}d^{n+1}\underline{L} = d^{n+1}\underline{L}^2d^{n+1}$ [65,66]. Thus, a considerable amount of O 2p states are present in the form of hybridization with the Ni 3d states at the E_F , schematically shown in Fig. 7(b), which effectively reduces the energy cost of transferring electron from O 2p states to unoccupied Ni 3d-O 2p hybridized state. Resultantly, the effective value of Δ decreases and hence O 2p hole along with Ni 3d electrons are participating in low-energy conduction process [18].

In $\text{LaNi}_{0.5}\text{V}_{0.5}\text{O}_3$ film, besides the presence of the incoherent structure at -1.5 eV, corresponding to the correlated localized V 3d electronic states, a coherent structure also appears at the lower-energy side of V 3d band corresponding

to the hybridized Ni $3d$ -O $2p$ band. In the CB, the first feature centered at +0.5 eV is also attributed to the Ni $3d$ -O $2p$ hybridized band. The tail of this band is extended to the E_F and consequently manifests a finite DOS at E_F as shown clearly in Fig. 7(a). Therefore, with the Ni doping in LVO, Ni $3d$ -O $2p$ hybridized states are emerging near across E_F . Such enhanced spectral DOS at E_F is an outcome of the enhanced bandwidth of the Ni $3d$ -O $2p$ hybridized band with Ni doping, which provides delocalized conduction electrons [19]. A sharp feature appearing at the +3.2 eV in CB of $\text{LaNi}_{0.5}\text{V}_{0.5}\text{O}_3$ film is due to the unoccupied V $3d$ band. It is important to note here that in $\text{LaNi}_{0.5}\text{V}_{0.5}\text{O}_3$ film the energy separation between occupied and unoccupied V $3d$ states, i.e., the energy difference between V $3d^1$ and V $3d^3$ electronic states, increases as compared to the LVO film. Moreover, due to the presence of Ni $3d$ -O $2p$ hybridized bands near the E_F , the energy required to transfer an electron from occupied O $2p$ state to unoccupied V $3d$ states decreases compared to LVO film as shown in Fig. 7(b). Such modulation in energy separation between different states with Ni doping in LVO would arise due to the modification in lattice parameter as observed in the crystal structure analysis. Although sufficient doping of Ni in LVO would lead to the emergence of delocalized coherent states at E_F , the existence of an intense incoherent state in $\text{LaNi}_x\text{V}_{1-x}\text{O}_3$ films suggests an overwhelming presence of correlation effects nearly localizing charge carriers. The schematics of the overall band structure as derived from these experimental observations are illustrated in Fig. 7(c), which exhibits a tale of evolution of bands from LaVO_3 to LaNiO_3 as Ni is doped in the system.

IV. DISCUSSION

Here, we have explored the insulator to metal transition with the substitution of Ni^{3+} at the place of V^{3+} in $\text{LaNi}_x\text{V}_{1-x}\text{O}_3$ thin films. Such homovalent substitution of the V with Ni in $\text{LaNi}_x\text{V}_{1-x}\text{O}_3$ thin films gives the possibility to explore the insulator to metal transition without involving any electron/hole doping in the system [22,24–26,48,68]. Therefore, it is expected that no charge transfer should take place between the transition-metal atoms, as is observed, since the formal charge states remain the same. This is in contrast to the cases where heterovalent substitutions ($\text{R}_{1-x}\text{A}_x\text{MO}_3$) lead to the formations of hole/electron states near the E_F and cause the MIT. Though the homovalent substitution does not alter the formal charge state, such modification may induce disorder and change the DOS near the E_F as well as the spectral shape [22]. These changes in the spectral shape embark on a possibility of phase separation/coexistence in the systems. However, the structural and spectroscopic data of the studied $\text{LaNi}_x\text{V}_{1-x}\text{O}_3$ thin films confirm the absence of any phase coexistence/separation. In these systems, the potential mismatch between the TM ions sites causes the redistribution of spectral weight across the E_F and drives the insulator to metal transition [24]. Therefore, the electronic structure study of these systems helps us to investigate the insulator to metal transition by realizing the various electronic parameters.

Due to the smaller value of U compared to Δ , the early transition-metal oxide compounds are classified in the Mott-Hubbard regime in contrast to the late-TMO compounds,

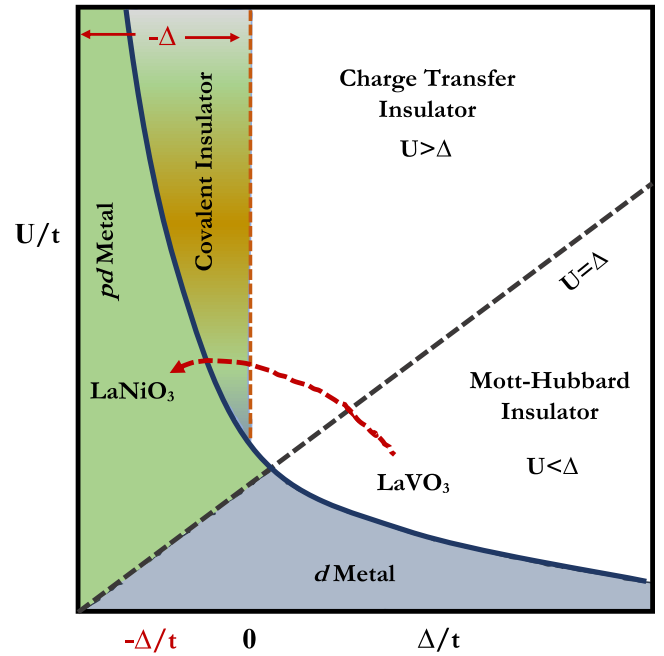


FIG. 8. Schematic representation of the transition from Mott-Hubbard insulating regime to negative Δ metallic regime with Ni doping in LVO film in U/t and Δ/t phase diagram.

which mainly fall in the charge transfer regime as the $U > \Delta$ [30]. Thus, the low-energy charge fluctuation in Mott-Hubbard insulator is of the type $d_i^n d_j^n \rightarrow d_i^{n-1} d_j^{n+1}$, while the same for the charge transfer insulator is $d_i^n d_j^n \rightarrow d_i^n d_j^{n+1} \underline{L}$. Moreover, in charge transfer insulator, if the Δ is small as compared to the metal ligand hybridization, then the weight of $d^{n+1} \underline{L}$ configuration becomes dominant in the ground state and can be classified as a negative Δ compound [5]. Rare-earth nickelates (RNiO_3) compounds are suggested to be placed in the negative Δ regime [19,66]. Though the insulating and metallic nature of negative Δ materials is strongly dependent on the strength of intercluster hybridization, resultant RNiO_3 shows MIT, except LNO [14,7,69]. The doping of late-TM element Ni in Mott-Hubbard insulator LVO does not lead to the carrier doping in $\text{LaNi}_x\text{V}_{1-x}\text{O}_3$ as observed in the electronic structure analysis; rather, the changes in ionic radius and consequent modification in crystal structure inherently lead to the modulation in bandwidth of TM-O $2p$ hybridized band. Generally, both the bandwidth-controlled and carrier-concentration controlled MIT are governed by the altering of electron correlation effect (U/W). However, the doping of Ni in LVO leads to a transition from the Mott-Hubbard insulating regime to negative Δ metallic regime, which has been controlled by the interplay between the U and Δ as shown schematically in Fig. 8. Therefore, unlike in Mott-Hubbard insulators where the strong Coulomb interaction between the d electrons decides the electronic structure and physical properties of the system, the properties of Ni-doped LVO films are governed by CT energy, which can provide an additional degree of freedom to optimize material properties. Moreover, the augmentation of Ni $3d$ spectral DOS in the Mott-Hubbard gap of insulating LVO with Ni doping offers an alternate pathway to study the interplay between the localized

and itinerant state of electron and tune the physical properties in a controlled experiment.

V. CONCLUSION

The electronic structure of $\text{LaNi}_x\text{V}_{1-x}\text{O}_3$ thin films grown on LaAlO_3 substrates has been analyzed employing the photoemission and absorption spectra at RT. The out-of-plane lattice parameter of grown films decreases with the Ni doping in LVO. Such Ni doping in Mott-Hubbard insulator LVO does not lead to the carrier doping in $\text{LaNi}_x\text{V}_{1-x}\text{O}_3$ films; rather, the modification in crystal structure leads to the modulation in bandwidth of TM $3d$ -O $2p$ hybridized band near E_F . The shift of Ni $3d$ -O $2p$ hybridized band towards higher energy in $\text{LaNi}_x\text{V}_{1-x}\text{O}_3$ films endorses the modification of

ligand to metal charge transfer energy. In sufficiently doped $\text{LaNi}_x\text{V}_{1-x}\text{O}_3$ films, besides the presence of incoherent structure, corresponding to the V $3d$ band essentially localized due to the electron correlation, a coherent structure also appears at the E_F corresponding to the hybridized Ni $3d$ -O $2p$ band which provides delocalized electrons for conduction. Our present work offers a spectroscopic realization of Mott-Hubbard insulator to negative Δ metal transition at RT.

ACKNOWLEDGMENTS

The authors acknowledge Rajeeb Rawat for the resistivity measurement. A.J. acknowledges Anita Bagri, Avinash Wadikar, Sharad Karwal, and Rakesh Sah, for helping in XRD, VBS, and XAS measurements.

-
- [1] G. H. Jonker and J. H. Van Santen, Ferromagnetic compounds of manganese with perovskite structure, *Physica* **16**, 337 (1950).
- [2] S. Jin, T. H. Tiefel, M. McCormack, R. A. Fastnacht, R. Ramesh, and L. H. Chen, Thousandfold change in resistivity in magnetoresistive La-Ca-Mn-O films, *Science* **264**, 413 (1994).
- [3] C. N. R. Rao, P. Ganguly, A. K. Raychaudhuri, R. A. Mohanram, and K. Sreedhar, Identification of the phase responsible for high-temperature superconductivity in Y-Ba-Cu oxides, *Nature (London)* **326**, 856 (1987).
- [4] N. F. Mott, The basis of the electron theory of metals, with special reference to the transition metals, *Proc. Phys. Soc. London, Sect. A* **62**, 416 (1949).
- [5] M. Imada, A. Fujimori, and Y. Tokura, Metal-insulator transitions, *Rev. Mod. Phys.* **70**, 1039 (1998).
- [6] A. Jana, R. J. Choudhary, and D. M. Phase, Mott-Hubbard type insulating nature of epitaxial LaVO_3 thin films, *Phys. Rev. B* **98**, 075124 (2018).
- [7] K. Sreedhar, J. M. Honig, M. Darwin, M. McElfresh, P. M. Shand, J. Xu, B. C. Crooker, and J. Spalek, Erratum: Electronic properties of the metallic perovskite LaNiO_3 : Correlated behavior of $3d$ electrons, *Phys. Rev. B* **47**, 5543(E) (1993).
- [8] P. Bordet, C. Chaillout, M. Marezio, Q. Huang, A. Santoro, S. W. Cheong, H. Takagi, C. S. Oglesby, and B. Batlogg, Structural aspects of the crystallographic-magnetic transition in LaVO_3 around 140 K, *J. Solid State Commun.* **106**, 253 (1993).
- [9] M. De Raychaudhuri, E. Pavarini, and O. K. Andersen, Orbital Fluctuations in the Different Phases of LaVO_3 and YVO_3 , *Phys. Rev. Lett.* **99**, 126402 (2007).
- [10] S. Miyasaka, T. Okuda, and Y. Tokura, Critical Behavior of Metal-Insulator Transition in $\text{La}_{1-x}\text{Sr}_x\text{VO}_3$, *Phys. Rev. Lett.* **85**, 5388 (2000).
- [11] S. Miyasaka, Y. Okimoto, M. Iwama, and Y. Tokura, Spin-orbital phase diagram of perovskite-type RVO_3 (R = rare-earth ion or Y), *Phys. Rev. B* **68**, 100406(R) (2003).
- [12] O. Müller, J. P. Urbach, E. Goering, T. Weber, R. Barth, H. Schuler, M. Klemm, S. Horn, and M. L. denBoer, Spectroscopy of metallic and insulating V_2O_3 , *Phys. Rev. B* **56**, 15056 (1997).
- [13] A. Jana, R. Raghunathan, R. Rawat, R. J. Choudhary, and D. M. Phase, Enhanced charge-transfer character in the monoclinic phase of Mott insulator LaVO_3 thin films, *Phys. Rev. B* **102**, 235108 (2020).
- [14] J. B. Torrance, P. Lacorre, A. I. Nazzari, E. J. Ansaldo, and C. Niedermayer, Systematic study of insulator-metal transitions in perovskites RNiO_3 (R = Pr, Nd, Sm, Eu) due to closing of charge-transfer gap, *Phys. Rev. B* **45**, 8209 (1992).
- [15] K. P. Rajeev, G. V. Shivashankar, and A. K. Raychaudhuri, Low-temperature electronic properties of a normal conducting perovskite oxide (LaNiO_3), *Solid State Commun.* **79**, 591 (1991).
- [16] J. B. Goodenough, Localized versus collective d electrons and Néel temperatures in perovskite and perovskite-related structures, *Phys. Rev.* **164**, 785 (1967).
- [17] K. M. Satyalakshmi, K. B. R. Varma, and M. S. Hedge, Ferroelectric properties of $\text{Bi}_2\text{VO}_{5.5}$ thin films on LaAlO_3 and SiO_2/Si substrates with LaNiO_3 base electrode, *J. Appl. Phys.* **78**, 1160 (1995).
- [18] S. R. Barman, A. Chainani, and D. D. Sarma, Covalency-driven unusual metal-insulator transition in nickelates, *Phys. Rev. B* **49**, 8475 (1994).
- [19] S. Middey, J. Chakhalian, P. Mahadevan, J. W. Freeland, A. J. Millis, and D. D. Sarma, Physics of ultrathin films and heterostructures of rare-earth nickelates, *Annu. Rev. Mater. Res.* **46**, 305 (2016).
- [20] H. T. Dang and A. J. Millis, Theory of ferromagnetism in vanadium-oxide based perovskites, *Phys. Rev. B* **87**, 155127 (2013).
- [21] H. Guo, Z. W. Li, L. Zhao, Z. Hu, C. F. Chang, C.-Y. Kuo, W. Schmidt, A. Piovano, T. W. Pi, O. Sobolev, D. I. Khomskii, L. H. Tjeng, and A. C. Komarek, Antiferromagnetic correlations in the metallic strongly correlated transition metal oxide LaNiO_3 , *Nat. Commun.* **9**, 43 (2018).
- [22] D. D. Sarma, A. Chainani, S. R. Krishnakumar, E. Vescovo, C. Carbone, W. Eberhardt, O. Rader, Ch. Jung, Ch. Hellwig, W. Gudat, H. Srikanth, and A. K. Raychaudhuri, Disorder Effects in Electronic Structure of Substituted Transition Metal Compounds, *Phys. Rev. Lett.* **80**, 4004 (1998).
- [23] C. N. R. Rao, O. Prakash, and P. Ganguly, Electronic and magnetic properties of $\text{LaNi}_{1-x}\text{Co}_x\text{O}_3$, $\text{LaCo}_{1-x}\text{Fe}_x\text{O}_3$ and $\text{LaNi}_{1-x}\text{Fe}_x\text{O}_3$, *J. Solid State Chem.* **15**, 186 (1975).
- [24] D. D. Sarma, O. Rader, T. Kachel, A. Chainani, M. Mathew, K. Holldack, W. Gudat, and W. Eberhardt, Contrasting behavior of homovalent-substituted and hole-doped systems: O

- K -edge spectra from $\text{LaNi}_{1-x}\text{M}_x\text{O}_3$ ($M = \text{Mn, Fe, and Co}$) and $\text{La}_{1-x}\text{Sr}_x\text{MnO}_3$, *Phys. Rev. B* **49**, 14238 (1994).
- [25] R. Kumar, R. J. Choudhary, M. W. Khan, J. P. Srivastava, C. W. Bao, H. M. Tsai, J. W. Chiou, K. Asokan, and W. F. Pong, Structural, electrical transport and x-ray absorption spectroscopy studies of $\text{LaFe}_{1-x}\text{Ni}_x\text{O}_3$ ($x < 0.6$), *J. Appl. Phys.* **97**, 093526 (2005).
- [26] P. Ganguly, N. Y. Vasanthacharya, C. N. R. Rao, and P. P. Edwards, Composition-controlled metal-insulator transitions and minimum metallic conductivity in the oxide systems $\text{LaNi}_{1-x}\text{M}_x\text{O}_3$ ($M = \text{Cr, Mn, Fe, or Co}$), *J. Solid State Chem.* **54**, 400 (1984).
- [27] J. A. Wilson, in *The Metallic and Nonmetallic States of Matter*, edited by P. P. Edwards and C. N. R. Rao (Taylor and Francis, London, 1985), p. 215.
- [28] I. H. Inoue, O. Goto, H. Makino, N. E. Hussey, and M. Ishikawa, Bandwidth control in a perovskite-type $3d^1$ -correlated metal $\text{Ca}_{1-x}\text{Sr}_x\text{VO}_3$. I. Evolution of the electronic properties and effective mass, *Phys. Rev. B* **58**, 4372 (1998).
- [29] Y. Okimoto, T. Katsufuji, Y. Okada, T. Arima, and Y. Tokura, Optical spectra in $(\text{La}, \text{Y})\text{TiO}_3$: Variation of Mott-Hubbard gap features with change of electron correlation and band filling, *Phys. Rev. B* **51**, 9581 (1995).
- [30] J. Zaanen, G. A. Sawatzky, and J. W. Allen, Band Gaps and Electronic Structure of Transition-Metal Compounds, *Phys. Rev. Lett.* **55**, 418 (1985).
- [31] K. M. Satyalakshmi, F. L. M. Mallya, K. V. Ramanathan, X. D. Wu, B. Brainard, D. C. Gautier, N. Y. Vasanthacharya, and M. S. Hegde, Epitaxial metallic LaNiO_3 thin films grown by pulsed laser deposition, *Appl. Phys. Lett.* **62**, 1233 (1993).
- [32] H. Rotella, U. Luders, P.-E. Janolin, V. H. Dao, D. Chateigner, R. Feyerherm, E. Dudzik, and W. Prellier, Octahedral tilting in strained LaVO_3 thin films, *Phys. Rev. B* **85**, 184101 (2012).
- [33] A. V. Mahajan, D. C. Johnston, D. R. Torgeson, and F. Borsa, Structural, electronic, and magnetic properties of $\text{La}_x\text{Sr}_{1-x}\text{VO}_3$ ($0.1 \leq x \leq 1.0$), *Phys. Rev. B* **46**, 10973 (1992).
- [34] A. R. Denton and N. W. Ashcroft, Vegard's law, *Phys. Rev. A* **43**, 3161 (1991).
- [35] J. Zhang, H. Zheng, Y. Ren, and J. F. Mitchell, High-pressure floating-zone growth of perovskite nickelate LaNiO_3 single crystals, *Cryst. Growth Des.* **17**, 2730 (2017).
- [36] H. H. Sønsteby, E. Skaar, Ø. S. Fjellvåg, J. E. Bratvold, H. Fjellvåg, and O. Nilsen, A foundation for complex oxide electronics -low temperature perovskite epitaxy, *Nat. Commun.* **11**, 1 (2020).
- [37] S. J. Gharetape, M. P. Sing, F. S. Razavi, D. A. Crandles, L. Y. Zhao, and K. T. Leung, Effect of vanadium deficiency on properties of polycrystalline LaVO_3 , *Appl. Phys. Lett.* **98**, 052509 (2011).
- [38] R. P. Gupta and S. K. Sen, Calculation of multiplet structure of core p -vacancy levels, II, *Phys. Rev. B* **12**, 15 (1975).
- [39] N. Kamakura, M. Taguchi, A. Chainani, Y. Takata, K. Horiba, K. Yamamoto, K. Tamasaku, Y. Nishino, D. Miwa, E. Ikenaga, M. Awaji, A. Takeuchi, H. Ohashi, Y. Senba, H. Namatame, M. Taniguchi, T. Ishikawa, K. Kobayashi, and S. Shin, Hard X-ray core-level photoemission of V_2O_3 , *Europhys. Lett.* **68**, 557 (2004).
- [40] R. Eguchi, M. Taguchi, M. Matsunami, K. Horiba, K. Yamamoto, A. Chainani, Y. Takata, M. Yabashi, D. Miwa, Y. Nishino, K. Tamasaku, T. Ishikawa, Y. Senba, H. Ohashi, I. H. Inoue, Y. Muraoka, Z. Hiroi, and S. Shin, Electronic structure of $3d^1$ configuration vanadium oxides studied by soft X-ray and hard X-ray photoemission spectroscopy, *J. Electron Spectrosc. Relat. Phenom.* **156**, 421 (2007).
- [41] M. Taguchi, A. Chainani, N. Kamakura, K. Horiba, Y. Takata, M. Yabashi, K. Tamasaku, Y. Nishino, D. Miwa, T. Ishikawa, S. Shin, E. Ikenaga, T. Yokoya, K. Kobayashi, T. Mochiku, K. Hirata, and K. Motoya, Bulk screening in core-level photoemission from Mott-Hubbard and charge-transfer systems, *Phys. Rev. B* **71**, 155102 (2005).
- [42] A. Kotani and Y. Toyozawa, Photoelectron spectra of core electrons in metals with an incomplete shell, *J. Phys. Soc. Jpn.* **37**, 912 (1974).
- [43] R. J. O. Mossaneck, M. Abbate, T. Yoshida, A. Fujimori, Y. Yoshida, N. Shirakawa, H. Eisaki, S. Kohno, and F. C. Vicentin, Evolution of the spectral weight in the Mott-Hubbard series SrVO_3 - CaVO_3 - LaVO_3 - YVO_3 , *Phys. Rev. B* **78**, 075103 (2008).
- [44] E. Stavitski and F. M. F. de Groot, The CTM4XAS program for EELS and XAS spectral shape analysis of transition metal L edges, *Micron* **41**, 687 (2010).
- [45] D. Ruzmetov, S. D. Senanayake, and S. Ramanathan, X-ray absorption spectroscopy of vanadium dioxide thin films across the phase-transition boundary, *Phys. Rev. B* **75**, 195102 (2007).
- [46] B. Chen, J. Laverock, D. Newby, Jr., J. F. McNulty, K. E. Smith, P.-A. Glans, F.-H. Guo, R.-M. Qiao, W.-L. Yang, M. R. Lees, L. D. Tung, R. P. Singh, and G. Balakrishnan, Effects of rare-earth size on the electronic structure of $\text{La}_{1-x}\text{Lu}_x\text{VO}_3$, *J. Phys.: Condens. Matter* **27**, 105503 (2015).
- [47] J. Laverock, B. Chen, A. R. H. Preston, K. E. Smith, N. R. Wilson, G. Balakrishnan, P.-A. Glans, and J.-H. Guo, Electronic structure of the kagome staircase compounds $\text{Ni}_3\text{V}_2\text{O}_8$ and $\text{Co}_3\text{V}_2\text{O}_8$, *Phys. Rev. B* **87**, 125133 (2013).
- [48] J.-S. Kang, H. J. Lee, G. Kim, D. H. Kim, B. Dabrowski, S. Kolesnik, Hangil Lee, J.-Y. Kim, and B. I. Min, Electronic structure of the cubic perovskite $\text{SrMn}_{1-x}\text{Fe}_x\text{O}_3$ investigated by x-ray spectroscopies, *Phys. Rev. B* **78**, 054434 (2008).
- [49] F. M. F. de Groot, J. C. Fuggle, B. T. Thole, and A. G. Sawatzky, $2p$ x-ray absorption of $3d$ transition-metal compounds: An atomic multiplet description including the crystal field, *Phys. Rev. B* **42**, 5459 (1990).
- [50] J. Zaanen, G. A. Sawatzky, J. Fink, W. Speier, and J. C. Fuggle, L_{2,3} absorption spectra of the lighter $3d$ transition metals, *Phys. Rev. B* **32**, 4905 (1985).
- [51] F. M. F. de Groot, M. Grioni, J. C. Fuggle, J. Ghijsen, G. A. Sawatzky, and H. Petersen, Oxygen $1s$ x-ray-absorption edges of transition-metal oxides, *Phys. Rev. B* **40**, 5715 (1989).
- [52] A. Abragam and B. Bleaney, *Electron Paramagnetic Resonance of Transition Ions* (Oxford University Press, Oxford, 1970), Chap. 16.
- [53] Y. Kumar, A. P. Singh, S. K. Sharma, R. J. Choudhary, P. Thakur, M. Knobel, N. B. Brookes, and R. Kumar, Irradiation induced modification in transport properties of LaNiO_3 thin films: An x-ray absorption study, *Appl. Phys. Lett.* **101**, 112103 (2012).
- [54] M. Hepting, D. Li, C. J. Jia, H. Lu, E. Paris, Y. Tseng, X. Feng, M. Osada, E. Been, Y. Hikita, Y.-D. Chuang, Z. Hussain, K. J. Zhou, A. Nag, M. Garcia-Fernandez, M. Rossi, H. Y. Huang, D. J. Huang, Z. X. Shen, T. Schmitt, H. Y. Hwang, B. Moritz, J. Zaanen, T. P. Devereaux, and W. S. Lee, Electronic structure

- of the parent compound of superconducting infinite-layer nickelates, *Nat. Mater.* **19**, 381 (2020).
- [55] M. Abbate, G. Zampieri, F. Prado, A. Caneiro, J. M. Gonzalez-Calbet, and M. Vallet-Regi, Electronic structure and metal-insulator transition in $\text{LaNiO}_{3-\delta}$, *Phys. Rev. B* **65**, 155101 (2002).
- [56] J. Chakhalian, J. M. Rondinelli, J. Liu, B. A. Gray, M. Kareev, E. J. Moon, N. Prasai, J. L. Cohn, M. Varela, I. C. Tung, M. J. Bedzyk, S. G. Altendorf, F. Strigari, B. Dabrowski, L. H. Tjeng, P. J. Ryan, and J. W. Freeland, Asymmetric Orbital-Lattice Interactions in Ultrathin Correlated Oxide Films, *Phys. Rev. Lett.* **107**, 116805 (2011).
- [57] M. Alexander, H. Romberg, N. Nucker, P. Adelman, J. Fink, J. T. Markert, M. B. Maple, S. Uchida, H. Takagi, Y. Tokura, A. C. W. P. James, and D. W. Murphy, Electronic structure studies on the n-type doped superconductors $R_{2-x}M_x\text{CuO}_{4-\delta}$ ($R = \text{Pr, Nd, Sm}$; $M = \text{Ce, Th}$) and $\text{Nd}_2\text{CuO}_{4-x}\text{F}_x$ by electron-energy-loss spectroscopy, *Phys. Rev. B* **43**, 333 (1991).
- [58] G. Van der Laan and I. W. Kirkman, The $2p$ absorption spectra of $3d$ transition metal compounds in tetrahedral and octahedral symmetry, *J. Phys.: Condens. Matter* **4**, 4189 (1992).
- [59] C. Suzuki, J. Kawai, M. Takahashi, A.-M. Vlaicu, H. Adachi, and T. Mukoyama, The electronic structure of rare-earth oxides in the creation of the core hole, *Chem. Phys.* **253**, 27 (2000).
- [60] M. Medarde, A. Fontaine, J. L. Garcia-Munoz, J. Rodríguez-Carvajal, M. de Santis, M. Sacchi, G. Rossi, and P. Lacorre, RNiO_3 perovskites ($R = \text{Pr, Nd}$): Nickel valence and the metal-insulator transition investigated by x-ray-absorption spectroscopy, *Phys. Rev. B* **46**, 14975 (1992).
- [61] K. Tsubouchi, I. Ohkubo, H. Kumigashira, Y. Matsumoto, T. Ohnishi, M. Lippmaa, H. Koinuma, and M. Oshima, Epitaxial growth and surface metallic nature of LaNiO_3 thin films, *Appl. Phys. Lett.* **92**, 262109 (2008).
- [62] K. Maiti and D. D. Sarma, Spectroscopic investigations of the electronic structure and metal-insulator transitions in a Mott-Hubbard system $\text{La}_{1-x}\text{Ca}_x\text{VO}_3$, *Phys. Rev. B* **61**, 2525 (2000).
- [63] S. Grebinkij, M. Senulis, H. Tvardauskas, V. Bondarenka, V. Lissauskas, K. Sliuziene, B. Vengalis, B. A. Orłowski, R. L. Johnson, and S. Mickevicius, Valence band study of $\text{LaNiO}_{3-\delta}$ thin films, *Radiat. Phys. Chem.* **80**, 1135 (2011).
- [64] R. Rawat, A. Jana, G. Panchal, S. Chowdhury, R. J. Choudhary, and D. M. Phase, Temperature driven Mott-Hubbard to charge-transfer insulator transition in hexagonal $\text{Sr}_{0.6}\text{Ba}_{0.4}\text{MnO}_3$, *Appl. Phys. Lett.* **115**, 102905 (2019).
- [65] S. Chowdhury, A. Jana, M. Kuila, V. R. Reddy, R. J. Choudhary, and D. M. Phase, Negative charge-transfer energy in $\text{SrCoO}_{2.5}$ thin Films: An interplay between O- $2p$ hole density, charge-transfer energy, charge disproportionation, and ferromagnetic ordering, *ACS Appl. Electron. Mater.* **2**, 3859 (2020).
- [66] V. Bisogni, S. Catalano, R. J. Green, M. Gibert, R. Scherwitzl, Y. Huang, V. N. Strocov, P. Zubko, S. Balandeh, J.-M. Triscone, G. Sawatzky, and T. Schmitt, Ground-state oxygen holes and the metal-insulator transition in the negative charge-transfer rare-earth nickelates, *Nat. Commun.* **7**, 13017 (2016).
- [67] E. Alves, H. P. Martins, S. Domenech, and M. Abbate, Band structure and cluster model calculations of LaNiO_3 compared to photoemission, O $1s$ X-ray absorption, and optical absorption spectra, *Phys. Lett. A* **383**, 2952 (2019).
- [68] D. H. Kim, H. J. Lee, B. Dabrowski, S. Kolesnik, J. Lee, B. Kim, B. I. Min, and J.-S. Kang, Photoemission spectroscopy study of metal-insulator transition in $\text{SrMn}_{1-x}\text{Fe}_x\text{O}_3$, *Phys. Rev. B* **81**, 073101 (2010).
- [69] T. Mizokawa, A. Fujimori, H. Namatame, K. Akeyama, and N. Kosugi, Electronic structure of the local-singlet insulator NaCuO_2 , *Phys. Rev. B* **49**, 7193 (1994).